PRAMANA
— journal of
physics

Vol. 73, No. 4
October 2009
pp. 669–683

Measurement and theoretical estimation of induced activity in ^{nat}In by high energy neutrons

MAITREYEE NANDY[1,*], P K SARKAR[2], N NAKAO[3] and T SHIBATA[3,4]
[1]Chemical Sciences Division, Saha Institute of Nuclear Physics, 1/AF, Bidhan Nagar, Kolkata 700 064, India
[2]ARSS, BARC & H.P. Unit, V.E.C. Centre, 1/AF, Bidhan Nagar, Kolkata 700 064, India
[3]Radiation Science Center, High Energy Accelerator Research Organisation, KEK, Tsukuba, Japan
[4]Present address: J-PARC Center, Japan Atomic Energy Agency, Tokai, Ibaraki, Japan
*Corresponding author. E-mail: maitreyee.nandy@saha.ac.in

MS received 20 January 2009; revised 29 April 2009; accepted 23 May 2009

Abstract. Induced radioactivity in natural indium (^{nat}In) foils by high energy neutrons was measured at the KENS Facility, KEK, Japan, where a 16.7 cm thick W target was bombarded by protons of 500 MeV. High energy neutrons consequently produced irradiated the In targets placed at different depths inside a 4 m thick concrete shield placed at the beam exit. The measured activities were compared with the results calculated using the nuclear reaction model codes ALICE-91 and EMPIRE-2.18. To estimate the induced activity, excitation functions of the various radionuclides were calculated using the two codes and folded with the appropriate neutron energy distribution at different depths of the concrete shield. The calculated excitation functions of a given nuclide were found to vary widely from one another in some cases. The performances of the codes for different input parameters like level densities and inverse cross-sections are reported in this paper. Our analysis shows that neither of the two codes reproduced all the measured activities satisfactorily, requiring further improvements in the models adopted.

Keywords. Induced activity; ALICE; EMPIRE; pre-equilibrium; excitation function.

PACS Nos 25.40.-h; 29.20.-c; 29.40.-n

1. Introduction

Experiments of fast neutron-induced reactions at intermediate energies (E_n = 20–200 MeV) has been for a long time kept aside because of specific experimental difficulties, in spite of their usefulness in many studies such as nuclear interaction mechanisms, radiation treatment of cancer, soft-error evaluation in computer memories, response of neutron detectors, etc. With the advent of the new accelerator-driven systems, considered for the transmutation of long-lived nuclear waste into shorter lived products, and for many other applications, there has been a renewed interest in nuclear data on neutron-induced reactions in this energy range. Integral

excitation functions for the production of residual nuclides are basic quantities for the calculation of radioactive inventories of spallation targets in spallation neutron sources and in accelerator-driven devices planned to be used for energy amplification or for transmutation of nuclear waste.

Such inventories help in proper planning of the facility, shield design, optimum use of the expensive beam time with proper planning of the experiment, protection of personnel and equipment, etc. These estimations may be carried out either through direct measurements or through model calculations of the characteristic variables defining the induced radioactivity. Considering the wide energy range spanned by the emitted neutrons resulting in the production of a large number of radioisotopes, it is not always feasible to carry out experimental measurements. This has led the practitioners in the field to put a high premium on the computational methods based on nuclear reaction model codes.

In the present work, radioactivity induced in natural indium (^{nat}In) targets, by neutrons produced from thick tungsten (W) target irradiated by 500 MeV protons and subsequently transported through different thicknesses of concrete was measured at KEK Neutron Scattering (KENS) Facility, KEK, Japan [1]. The measured activities were compared with the values calculated with the nuclear reaction model codes ALICE-91 [2] and EMPIRE-2.18 [3] and the performance of the codes analysed. For the computational part, we concentrate on a systematic survey on the phenomenology of excitation functions for the indium (^{113,115}In) target and present some tests of models and codes describing medium-energy nuclear reactions. Natural In has been widely used as a threshold activation foil for fluence monitoring of low energy (epithermal) neutrons using the (n, γ) reaction mechanism. In this work we wish to explore the possibility of its use as a threshold detector in higher energy range using (n, xn) reactions.

In §2 we briefly describe the experiment and in §3 descriptions of the nuclear reaction models and codes used are given. In §4 we report and discuss the results of our study.

2. Experimental details

500 MeV protons of 5 μA beam-current intensity from the 500 MeV proton accelerator at the KENS Facility, KEK, Japan was allowed to be incident on a 16.7 cm thick tungsten target where it was completely stopped. Neutrons produced from this interaction travelled through a rectangular collimator (20 cm width $\times$ 15 cm height) and reached the 4 m thick concrete shield placed in contact with the beam exit at a distance of 2.5 m from the W target. These neutrons irradiated the In foils and discs placed at different slots (sample insertion tubes) located at different depths inside the concrete shield. A schematic view of the experimental arrangement is shown in figure 1. In a rectangular slot (slot 1) in the front surface of the shield and in six cylindrical slots of 10.6 cm diameter (slots 2–7) inside the shield, shielding plugs filled with the same concrete were inserted during the experiment. Acryl capsules containing irradiation samples can be attached at the bottom of the plugs, and then placed on the beam axis inside the shield from the top of the target station. Slot 8 is located at the 4-m-thick shield end.

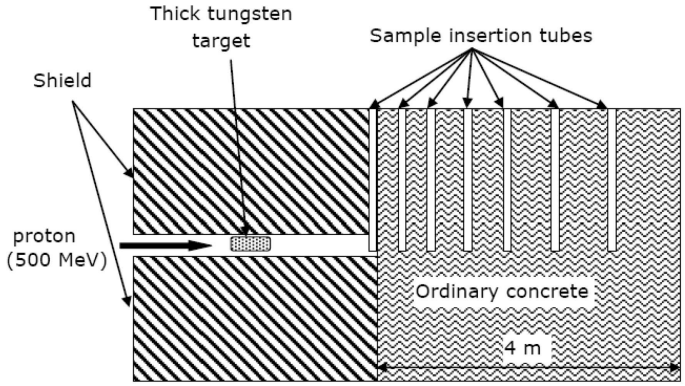

Figure 1. Schematic view of the experimental arrangement. The four sample insertion tubes from extreme left, i.e. nearest to the target, define slots 1, 2, 3, 4 and contain indium foils IF1, IF2, IF3 and IF4. The last four sample insertion tubes shown in figure contain thin indium discs IX4, IX5, IX6 and IX7. Slot 8 is at the end of 4 m thick concrete shield (extreme right) (not shown in figure) and contains the thick indium disc IN8.

In slot 1 the sample foil is exposed to direct source neutrons with no concrete in between, whereas in slot 2 the neutrons are transmitted through 40 cm of concrete before irradiating the foil. The position of the In foils (IF) and discs (IX and IN), and their dimensions are shown in table 1. The foils irradiated at different slots are identified as IF followed by the slot number. Similarly, thin and thick discs are identified as IX and IN respectively, followed by the slot number. The shape of the energy distribution of neutrons is different at different slots. The neutron spectra at different slot positions are shown in figure 2. It is seen that the neutron fluence has reduced by about five orders of magnitude (i.e. factor of 10^5) from slot 1 to slot 8. Because of this drastic reduction of neutron intensity, the weight, thickness as well as overall dimensions of the target were increased with increasing slot number to obtain good counting statistics while estimating the induced activity.

The In targets were removed after seven days of irradiation and were analysed using a HP-Ge detector for gamma spectrometry and subsequent quantitative estimation of the radionuclides formed in In target due to neutron-induced reactions. Efficiency calibration of the detector was done using gamma sources of known strengths. Then Monte Carlo simulations were carried out using source geometries corresponding to the above sources as well as for foils, thin discs and large discs. The calculated results were normalized using the measured data to obtain the efficiency factors corresponding to the different shapes. The calculated results also give relevant self-attenuation factors as the radioactivity was assumed to be uniformly distributed in the foils or discs.

Table 2 gives the radionuclides produced that can be identified by the emitted γ energies along with their branching ratios and half-lives. Each In target was counted repeatedly after different decay times in order to follow and ascertain the half-lives of the radionuclides formed wherever possible. In the first slot the foil was exposed to source neutrons from 500 MeV protons on thick W. The induced activity

Table 1. Specifications and positions of In foils and discs placed at different slots. Slot numbers start from extreme left sample insertion tube (nearest to the target).

Slot number	Interposed concrete thickness (cm)	Foil (square) Weight = 0.08 g, size (mm) = $10 \times 10 \times 0.1$ Identification number	Disc (thin) weight = 4.5 g, dia. = 20 mm, thickness = 2 mm Identification number	Disc (thick) Weight = 365 g, dia. = 80 mm, thickness = 10 mm Identification number
1	0.0	IF1		
2	40.0	IF2		
3	80.0	IF3		
4	130.0	IF4	IX4	
5	185.0		IX5	
6	250.0		IX6	
7	320.0		IX7	
8	400.0			IN8

in the In target due to a particular radionuclide after seven days of irradiation was then determined by introducing corrections due to detector efficiency, decay during irradiation, cooling and counting.

3. Reaction model calculation

In an attempt to theoretically estimate the neutron-induced activity in In targets using nuclear reaction models and to evaluate the performance of the nuclear reaction model codes available in the concerned energy range, the induced activity in In was calculated using the nuclear reaction model codes ALICE-91 [2] and EMPIRE-2.18 [3]. Production cross-sections of different radionuclides from neutron-induced reactions in the two naturally occurring isotopes of In (^{115}In, 95.71% and ^{113}In, 4.29%) were calculated for incident neutron energies up to 200 MeV. This upper limit was selected because the production cross-sections become small around this energy and smaller afterwards, and secondly, the codes are not expected to work properly beyond this energy.

The final production cross-sections of the radionuclides were computed from the weighted sum of the results from ^{115}In and ^{113}In in appropriate percentages. The production cross-sections thus calculated were folded with the neutron fluence distributions over the entire energy range, integrated over energy and multiplied by the number of target atoms available for the reaction to obtain the total yield of the radionuclide. The neutron fluence distributions at different slot positions were taken from an earlier reported work on the same experiment where calculations were done using the MARS code [1]. Induced activity due to a particular radionuclide after seven days of irradiation was then determined by taking into account the decay rate, the corrections due to decay during irradiation.

Table 2. Observed γ energies (keV) and the corresponding radionuclides with their half-lives and branching ratios (%). The data are taken from *Radioisotope Pocket Data Book*, 10th edn, JRIA.

Gamma energy (keV)	Radionuclides	Half-life	Branching ratio (%)
138	^{116m}In	54.41 min	3.3
171	^{111}In	2.805 d	90.2
190	^{114m}In	49.5 d	15.6
204	^{109}In	4.2 h	73.5
245	^{111}In	2.805 d	94.0
336	^{115m}In	4.486 h	45.8
	^{115}Cd	53.46 h	45.9
417	^{116m}In	54.41 min	27.7
558	^{114m}In	49.5 d	3.2
658	^{110}In	4.9 h	98.3
	^{110m}Ag	249.8 d	94.0
819	^{116m}In	54.41 min	11.5
885	^{110}In	4.9 h	92.9
	^{110m}Ag	249.8 d	94.0
937	^{110}In	4.9 h	68.4
1097	^{116m}In	54.41 min	56.2
1294	^{116m}In	54.41 min	56.2
1507	^{116m}In	54.41 min	56.2

3.1 *ALICE*-91

The code ALICE-91 [2,4] calculates pre-equilibrium (PEQ) emission of nucleons using the hybrid model followed by compound nuclear or equilibrium (EQ) emission of protons, neutrons, α-particles and deuterons using the Weisskopf–Ewing formalism. It considers PEQ emission of single neutron, single proton and simultaneously of two nucleons (p–p, p–n, n–n). PEQ emission of the cluster is not included. In its mode of following the relaxation process, the hybrid model combines the Boltzmann master equation and the exciton model. Each stage of the relaxation process is characterized by the exciton number (n) as in the closed form of the exciton model, i.e., using the 'never-come-back' approximation, i.e., each two-body interaction is assumed to increase n to $(n+2)$. However, instead of assuming an equal *a priori* probability for all energy distributions, the hybrid model explicitly evaluates the pre-emission energy distribution of the ejectile of interest in terms of appropriate intermediate partial state densities at each stage of the relaxation process. The hybrid model calculates the PEQ energy spectra of nucleon from a closed form expression. The code has provision to use different formalisms for the level density of residual nuclides which determine the probability of EQ emission and different formulation for the cross-section of the reverse channel (inverse cross-section). In the present work we have used different combinations of level density formalisms (Fermi gas and Gilbert–Cameron) and inverse cross-sections calculated using the sharp cut-off and the optical model which are described later.

3.2 *EMPIRE*-2.18

EMPIRE is a modular system of nuclear reaction codes [3], comprising various nuclear reaction models and designed for calculations over a broad range of energies and incident particles. A projectile can be a neutron, proton, any ion (including heavy ions), or a photon. The energy range extends from a few keV for neutron-induced reactions to several hundreds of MeV for heavy-ion-induced reactions. The code accounts for the major nuclear reaction mechanisms, including direct (DIR), PEQ and EQ ones. The compound nucleus decay is described by the Hauser–Feshbach model with γ-cascade and width fluctuations. The statistical model used in EMPIRE is an advanced implementation of the Hauser–Feshbach theory. The exact angular momentum and parity coupling are observed using l-dependent transmission coefficients. The emission of neutrons, protons, α-particles and a light ion is taken into account along with the competing fission channel. Angular distributions of particles emitted from the compound nucleus are assumed to be isotropic. The full γ cascade in the residual nuclei is considered. Determination of the level densities can be carried out in the non-adiabatic approach allowing for the rotational and vibrational enhancements. These collective effects are gradually removed above a certain energy. Level densities acquire dynamic features through the dependence of the rotational enhancement on the shape of the nucleus. In the frame of the statistical model of nuclear reactions, the contribution of the compound nucleus (CN) state with certain spin, parity and excitation energy to a channel is given by the ratio of the channel width to the total width multiplied by the population of this state. This also holds for secondary CNs that are formed due to subsequent particle emission. The only difference is that although the first CN is initially excited to the unique (incident channel compatible) energy, the secondary CNs are created with excitation energies that spread over the available energy interval. Each such state contributes to the cross-section.

4. Results and discussion

The projected range of 500 MeV protons in W is 11.11 cm [5] and the incident protons were completely stopped inside the 16.7 cm thick W target. The neutron spectra at each of the eight slots spanning the depth of 0–400 cm were calculated by MARS code in an earlier work [1], where the angular and energy distributions of neutrons produced from the tungsten target assembly bombarded by 500 MeV protons were calculated first. Then using the forward neutron spectrum as a source term, a neutron transmission calculation through 4-m-thick concrete was performed down to thermal energy. Energy modification and loss of neutrons due to straggling and secondary reaction were considered while calculating the neutron fluence distributions at various depths inside the concrete shield. The γ spectra of different radionuclides produced by the interaction of these neutrons with the ^{nat}In targets were recorded and the yields of different radionuclides were estimated.

Formation of ^{111}In is observed at all depths inside the concrete. ^{110}In+^{110}Ag are seen in slots 1, 2 and 4. ^{109}In is seen only in the first slot. ^{109}In is formed from ^{115}In(n,7n) and ^{113}In(n,5n) reactions and the yield of the isotope is observed to be

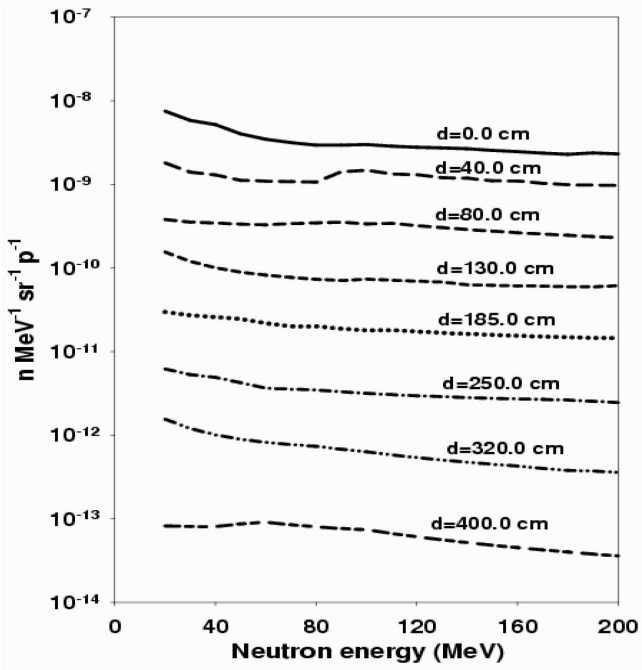

Figure 2. Neutron spectra from 500 MeV p+W reaction at different depths (d) in the concrete shield.

low. Moreover, it has a half-life of 4.2 h only. Hence the isotope could be detected only in the first slot just after the end of irradiation. As only one set of data is available, no further analysis is attempted.

As for the other isotopes shown in table 2, the yield of ^{116m}In is low since most of it is formed above the particle emission threshold and hence feed to other reaction channels. Moreover, it has a half-life of 54.41 min, hence could not be detected. In the case of ^{115}In and ^{115m}Cd, the yields are low, γ abundances are below 50% and they are emitting the same γ line. For ^{114}In, γ abundances are very low and statistics was poor.

Self-attenuation of 171, 245, 658 and 885 keV γ-rays is between 32 and 7% which has been taken into account in estimating the induced activity.

In the present work, we have studied the formation of the following radionuclides: (i) ^{111}In from ^{115}In(n,5n), ^{113}In(n,3n); (ii) ^{110}In from ^{115}In(n,6n), ^{113}In(n,4n); and (iii) ^{110}Ag from ^{115}In(n,4n2p), ^{115}In(n,α2n), ^{113}In(n,2n2p), ^{113}In(n,α).

In order to identify the radionuclides formed, the half-lives of the radionuclides were calculated from the measured activities by calculating their ratios after different decay times. For that purpose, the following formulation was used, which was solved iteratively using the Newton–Raphson's method:

$$\frac{C_1}{C_2}\exp[-\lambda(t_2-t_1)] = \frac{1-\exp(-\lambda t_{c1})}{1-\exp(-\lambda t_{c2})}, \tag{1}$$

where C_1 = counts under the peak after a decay time of t_1 and for counting time

t_{c1}, C_2 = counts under the peak after a decay time of t_2 and for counting time t_{c2} and λ = radioactive decay constant (=0.693/half-life).

Solving eq. (1) we have obtained a half-life of 2.7 days for ^{111}In and 4.15 h for ^{109}In. In the case of ^{110}In the situation was more complex because of the contribution of the gammas of the same energy (658 and 885 keV) from ^{110}Ag also. Here we have used the half-lives of the two isotopes from literature and determined the fractional contribution of each of the two radionuclides (^{110}In and ^{110}Ag) by using the following formulation:

$$\frac{C_1}{C_2} = \frac{\{f\exp(-\lambda_a t_1)[1-\exp(-\lambda_a t_{c1})]\}/\lambda_a + \{(1-f)\exp(-\lambda_b t_1)[1-\exp(-\lambda_b t_{c1})]\}\lambda_b}{\{f\exp(-\lambda_a t_2)[1-\exp(-\lambda_a t_{c2})]\}/\lambda_a + \{(1-f)\exp(-\lambda_b t_2)[1-\exp(-\lambda_b t_{c2})]\}\lambda_b}, \quad (2)$$

where C_1 = counts under the peak after a decay time of t_1 and for counting time t_{c1}, C_2 = counts under the peak after a decay time of t_2 and for counting time t_{c2}, λ_a, λ_b = radioactive decay constants for the radionuclides a and b respectively, f is the fractional contribution of the radionuclide a and this is determined from the above equation. The estimated percentage of radionuclides of ^{110}In is around 30% of the total (^{110}In+^{110}Ag).

4.1 *Calculation of production cross-sections*

Energy differential production cross-sections of ^{111}In, ^{110}In, ^{109}In and ^{110}Ag from ^{115}In and ^{113}In were calculated using the nuclear reaction model codes ALICE-91 and EMPIRE-2.18 for incident neutron energies in the range 1 MeV to 200 MeV.

In using ALICE-91, the geometry-dependent version of the hybrid model (GDH) was used to consider the effect of the diffuse nuclear surface. Four different combinations of the level density formalism and the reaction cross-section for the reverse channel were used which are mentioned below:

(a) Level density: Fermi gas, inverse cross-section: sharp cut-off (A-sfg).
(b) Level density: Fermi gas, inverse cross-section: optical model (A-ofg).
(c) Level density: Gilbert–Cameron, inverse cross-section: sharp cut-off (A-sgc).
(d) Level density: Gilbert–Cameron, inverse cross-section: optical model (A-ogc).

Evaporation was always calculated using the Weisskopf–Ewing formalism.

The modular code EMPIRE-2.18 was used with different combinations of PEQ reaction mechanisms like the multistep direct (MSD), multistep compound (MSC) and the Monte Carlo simulation of the hybrid model (HMS). The inverse cross-section was always calculated using the optical model. The combinations of the PEQ models and level density formalisms used with EMPIRE-2.18 are as follows:

(a) PEQ: MSD + MSC, level density: BCS + Fermi gas with deformation-dependent collective effects, inverse cross-section: optical model (E-msd+msc0).

(b) PEQ: Monte Carlo hybrid model (HMS), level density: BCS + Fermi gas with deformation-dependent collective effects, inverse cross-section: optical model (E-hms0).

(c) PEQ: HMS, level density: microscopic (Hartree–Fock) HF + BCS, inverse cross-section: optical model (E-hms3).

Table 3 shows the comparison between the measured and calculated activity of ^{111}In at the end of seven days of irradiation. It also gives the ratio of C/E (calculated/experimental) for the induced activity of ^{111}In. Here we see that the measured activity at the first slot is grossly underpredicted by all the model calculations while for the other slots the closest agreement is given by ALICE-91 calculation using the optical model inverse cross-section and Fermi gas level density. The HMS model in EMPIRE-2.18 gives a better agreement with the experimental data than the MSD+MSC calculations. Table 4 gives the combined activity of ^{110}In + ^{110}Ag obtained from experimental measurement and calculations, along with the C/E ratio. Here again we see that the measured activity in the first slot is grossly underpredicted by all the model calculations. For the other slots the same trend as in the case of ^{111}In is observed. The underprediction of experimental data for the first slot may be explained from the fact that more number of high energy neutrons are available in the first slot which may induce non-equilibrium (NEQ = Direct + PEQ) multiparticle emission. But none of the codes consider direct emission and PEQ emission is restricted either to single or double nucleons.

In order to further investigate the disagreement between different model calculations, we have plotted the results of model calculations for the excitation functions of ^{111}In, ^{110}In, ^{110}Ag and ^{109}In from neutron-induced reactions in ^{nat}In in figures 3–6. Large differences among the calculated results of the production cross-section of a radionuclide were observed for different models and input options selected. The plots of the calculated excitation functions are shown to indicate the variations in results from different codes.

For the production of ^{111}In from ^{nat}In the cross-section peaks at around 60.0 MeV of the incident neutron energy where the observed discrepancies are the largest. In this case, ALICE with Fermi gas level density and sharp cut-off inverse cross-sections (A-sfg) gives the highest cross-section (about 520 mb), whereas ALICE with Gilbert–Cameron level density and optical model inverse cross-sections (A-ogc) gives the lowest cross-section (about 90 mb). Among the ALICE results, the sharp cut-off inverse cross-sections give higher values of the production cross-section compared to the optical model inverse cross-sections, whereas the Gilbert–Cameron level density yields lower production cross-sections of ^{111}In from ^{nat}In. For EMPIRE-2.18 results, where the inverse cross-sections used are always from optical model calculations, the MSD + MSC model incorporating BCS + Fermi gas level density with deformation-dependent collective effects (E-msd+msc0) gives the lowest production cross-section. The HMS model incorporating microscopic Hartree–Fock (HF) + BCS level density option (E-hms3) gives the highest production cross-section followed by the HMS model using BCS + Fermi gas level density with deformation-dependent collective effects (E-hms0). We can observe similar trends for the production of ^{110}In and ^{109}In from ^{nat}In except for the fact that for ^{110}In ALICE calculations with Fermi gas level density and sharp cut-off inverse cross-sections (A-sfg) give a peak in the production cross-section around 50 MeV neutron energy, while ALICE with Fermi gas level density and optical model inverse cross-sections (A-ofg), EMPIRE with HMS and (Hartree–Fock) HF + BCS level density option (E-hms3) and EMPIRE with HMS and BCS+ Fermi gas level density with deformation-dependent collective effects (E-hms0) all give a peak in

Table 3. Experimentally measured and calculated values of the induced activity of ^{111}In in different slots. The (C/E) values for the calculated results are in parenthesis.

	Activity (dps) (C/E)							
Foil/disc	Experiment	A-ofg	A-ogc	A-sfg	A-sgc	E-hms0	E-hms3	E-msd +msc0
IF1	3061.7 ± 55	860 (0.28)	238 (0.08)	992 (0.32)	370 (0.12)	510 (0.17)	616 (0.20)	146 (0.05)
IF2	489.2 ± 22	266 (0.54)	71 (0.14)	309 (0.63)	111 (0.23)	170 (0.35)	205 (0.42)	39 (0.08)
IF3	79.1 ± 9	71 (0.89)	18 (0.23)	82 (1.03)	29 (0.37)	44 (0.56)	53 (0.67)	10 (0.13)
IF4	17.4 ± 4	17 (0.95)	4 (0.26)	19 (1.10)	7 (0.40)	10 (0.58)	12 (0.69)	3 (0.15)
IX4	1348.4 ± 37	1041 (0.77)	282 (0.21)	1203 (0.89)	441 (0.32)	633 (0.46)	755 (0.56)	169 (0.12)
IX5	250.4 ± 16	271 (1.08)	72 (0.29)	313 (1.25)	113 (0.45)	163 (0.65)	197 (0.78)	43 (0.17)
IX6	37.2 ± 6	43 (1.15)	12 (0.32)	49 (1.32)	18 (0.48)	26 (0.70)	31 (0.83)	7 (0.19)
IX7	4.9 ± 2	10 (2.04)	3 (0.61)	11 (2.24)	4 (0.82)	6 (1.22)	7 (1.42)	2 (0.40)
IN8	21.9 ± 5	81 (3.69)	21 (0.96)	93 (4.25)	33 (1.50)	48 (2.19)	60 (2.74)	13 (0.59)

Table 4. Experimentally measured and calculated values of the induced activity of $^{110}In + ^{110}Ag$ in different slots. The (C/E) values for the calculated results are in parenthesis.

Foil/ disc	Activity (dps) (C/E)							
	Exp.	A-ofg	A-ogc	A-sfg	A-sgc	E-hms0	E-hms3	E-msd +msc0
IF11	1335.1 ± 37	605.3 (0.45)	27.6 (0.02)	647.1 (0.48)	51.7 (0.04)	217.8 (0.16)	367.3 (0.28)	44.5 (0.03)
IF12	149.8 ± 12	207.2 (1.38)	8.6 (0.06)	219.8 (1.47)	16.2 (0.11)	81.0 (0.54)	133.3 (0.89)	13.2 (0.09)
IX14	782.1 ± 28	756.1 (0.97)	32.9 (0.04)	807.6 (1.03)	62.1 (0.08)	274.1 (0.35)	458.6 (0.59)	52.7 (0.07)
IX15	103.0 ± 10	197.0 (1.91)	8.5 (0.08)	210.5 (2.04)	16.1 (0.16)	70.9 (0.69)	119.8 (1.16)	14.0 (0.14)
IX16	19.5 ± 4.4	31.0 (1.59)	1.4 (0.07)	33.1 (1.70)	2.6 (0.13)	11.2 (0.57)	18.8 (0.97)	2.2 (0.11)

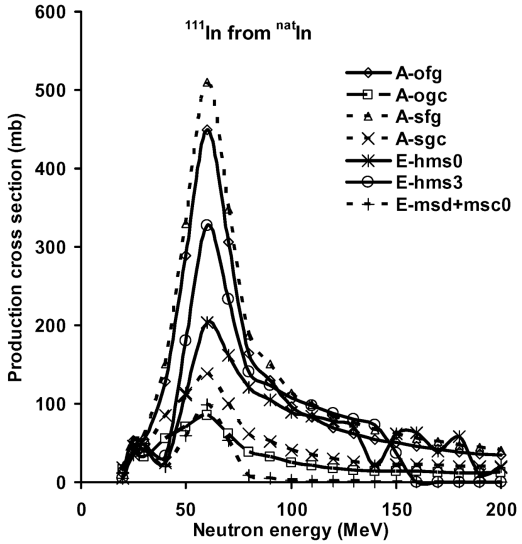

Figure 3. Production cross-sections of ^{111}In from ^{nat}In at different incident neutron energies calculated using ALICE and EMPIRE codes with different input options.

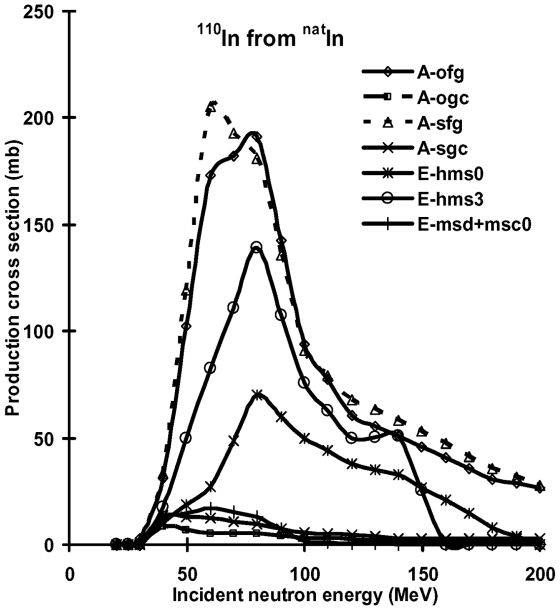

Figure 4. Production cross-sections of ^{110}In from ^{nat}In at different incident neutron energies calculated using ALICE and EMPIRE codes with different input options.

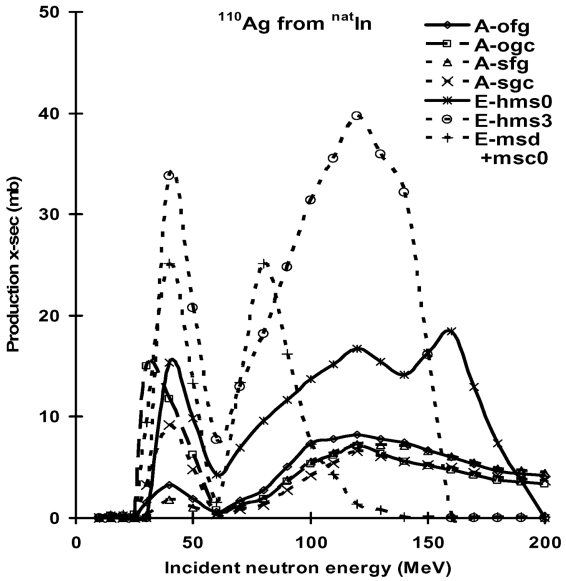

Figure 5. Production cross-sections of ^{110}Ag from ^{nat}In at different incident neutron energies calculated using ALICE and EMPIRE codes with different input options.

production cross-section around about 80 MeV. For other input options there are no discernable peak and the cross-sections are small comparatively. For ^{109}In the production cross-section peaks around 60 MeV for results from ALICE with Fermi gas level density and optical model inverse cross-sections (A-ofg), whereas for A-sfg, A-sgc and E-hms3 the peak is around 80 MeV.

The situation is complex for the production of ^{110}Ag from ^{nat}In, which can be produced through different channels like ^{115}In(n,4n2p) or ^{115}In(n,α2n), and ^{113}In(n,2n2p) or ^{113}In(n,α). Large discrepancies are observed for different codes and different input options. In this case, EMPIRE with HMS and HF+BCS level density option (E-hms3) gives the largest production cross-sections followed by EMPIRE with the MSD + MSC model incorporating BCS + Fermi gas level density with deformation-dependent collective effects (E-msd + msc0), which gave consistently low production cross-sections for ^{111,110,109}In isotopes. Results from ALICE show that in this case Gilbert–Cameron level density option gives higher values of the production cross-section compared to the Fermi gas level density option.

The difference among the theoretically computed results using ALICE is more pronounced when two different level density formalisms are used. This was particularly so when the product nuclei are far away (in charge and mass number) from the composite nucleus. Differences between ALICE-91 and EMPIRE-2.18 results could be attributed to the difference in the evaporation models used. However, difference among the two PEQ models used in EMPIRE-2.18 suggested a strong influence of PEQ emission mechanism in the production cross-sections. In the case of ^{110}Ag which can be formed by multiple nucleon emissions (4n2p from ^{116}In, 2n2p from

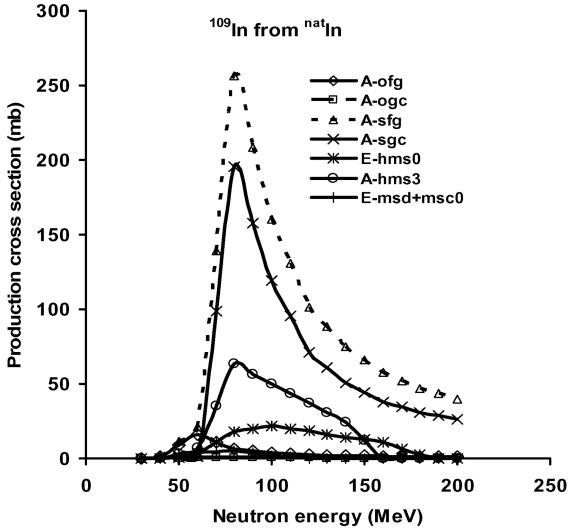

Figure 6. Production cross-sections of ^{109}In from ^{nat}In at different incident neutron energies calculated using ALICE and EMPIRE codes with different input options.

^{114}In) or by α + neutron emissions (α,2n from ^{116}In, α from ^{114}In), a significant difference in the shape of the curves is also observed. This study shows that optical model cross-section along with Fermi gas level density formalism is the best choice for such calculations.

5. Conclusions

Using the measured radioactivity induced in ^{nat}In by medium-energy neutrons we have analysed the energy differential production cross-sections of ^{111,110,109}In and ^{110}Ag. From the measured data of integral quantities it is not possible to have a detailed analysis of differential quantities. Nevertheless, it gives a useful overview particularly in the absence of mono-energetic neutron sources throughout this energy range. It may be noted that the codes used in the present analysis have not been rigorously studied for energies above 50 MeV. Excitation functions of residual nuclides for proton-induced reaction on different targets calculated with ALICE-IPPE (modified version of ALICE) have been compared with the measured data in the energy range upto 80 MeV by some workers. But ALICE-91 or earlier versions (ALICE-87) are used in a few works [6–8] for estimation and analysis of excitation functions in the energy range 90–110 MeV. EMPIRE-2.18 is not yet extensively used. Activation studies carried out using this code is mostly at much lower energies than 200 MeV as mentioned by the authors of the code in [3]. In order to use ALICE-91 and EMPIRE-2.18 to estimate excitation functions and induced activity in the energy region up to about 200 MeV, it can be concluded that multiparticle (more than two particles) PEQ emission needs to be incorporated in the models.

The phenomenology and energy dependence of the excitation functions exhibits clearly distinguishable reaction modes and demonstrates the necessity for further improvements of models and codes if medium-energy activation cross-sections for applications shall be reliably predicted by the theory.

Acknowledgement

The authors thankfully acknowledge the help of Dr T Sanami (formerly of KEK, Tsukuba, Japan), for providing HPGe detector and suggestions during the experiment.

References

[1] N Nakao *et al*, *Rad. Prot. Dosim.* **116**, 553 (2005)
[2] M Blann, Lawrence Livermore National Laboratory Report UCID 19614 (1982); ICTP Workshop Report No. SMR/284-1 (1988)
[3] M Herman, EMPIRE-II statistical model code for nuclear reaction calculations (2.18 Mondovi), IAEA, Vienna, Austria (2002)
M Herman *et al*, *Nucl. Data Sheets* **108**, 2655 (2007)
[4] M Blann, *Phys. Rev. Lett.* **27**, 337 (1971)
M Blann, *Phys. Rev. Lett.* **27**, 700E (1971)
[5] J F Ziegler, J P Biersack and U Littmark, *The stopping and range of ions in solids* (Pergamon Press, New York, 1985)
[6] N V Kurenkov, V P Lunev, V S Masterov and Yu N Shubin, *Appl. Radiat. lsot.* **46**, 29 (1995)
[7] E G Aydın, E Tel, A Kaplan and Ab Aydın, *Ann. Nucl. Energy* **35**, 2306 (2008)
[8] Maitreyee Nandy and P K Sarkar, *Appl. Radiat. Isot.* **54**, 101 (2001)